RSC Advances

PAPER

View Article Online
View Journal | View Issue

Open Access Article. Published on 23 February 2017. Downloaded on 10/25/2025 7:37:09 PM.
This article is licensed under a Creative Commons Attribution 3.0 Unported Licence.

Cite this: *RSC Adv.*, 2017, **7**, 12738

V_xO_y@C catalyst prepared from biomass for hydroxylation of benzene to phenol with molecular oxygen†

Weitao Wang,* Leilei Shi, Na Li and Yangmin Ma*

Received 28th December 2016
Accepted 10th February 2017

DOI: 10.1039/c6ra28768a

rsc.li/rsc-advances

A series of V_xO_y@C catalysts was prepared from different types of biomass and NH_4VO_3 using a hydrothermal method. The prepared catalysts were characterized using a series of methods including XRD, SEM, FT-IR, SEM and XPS to investigate the mechanism of formation of the V_xO_y@C catalysts. Furthermore, the factors related to the selectivity of phenol and the mechanism of the hydroxylation of benzene to phenol were studied. It was found that the activity was related to the V species on the catalyst and the selectivity was related to the adsorption of phenol.

Introduction

C–H bond activation is important in catalysis, especially the C–H bond of arenes. The C–H bond of benzene has a high binding energy of 473.1 kJ mol^{-1} at 298 K.[1] The functionalization of benzene is vitally important for the green conversion of benzene to other chemicals such as the direct conversion of benzene to phenols, anilines, *etc.*[2,3] However, functionalized benzene derivatives are thermodynamically and kinetically favorable to being further converted compared with benzene,[4,5] which makes the direct conversion of benzene to phenol or aniline a great challenge.

The direct conversion of benzene to phenol has attracted much research interest for it is a greener route than the industrial three steps of the cumene process route.[6–10] Direct conversion of benzene to phenol requires oxidant agents. Among the oxidant agents (such as H_2O_2, O_2 and N_2O) for the hydroxylation of benzene to phenol, O_2 is believed to be the most conveniently available and low cost oxidant. Much effort has been made to produce phenol by hydroxylation of benzene with molecular oxygen under mild conditions.[11–17] However, the mechanism and the factors affecting the selectivity are still not clear for the hydroxylation of benzene to phenol in the liquid phase. With H_2O_2 as the oxidant agent, C=O and the armchair configuration defects in the carbon catalyst were reported to have a positive effect on the yield of phenol.[18–20] However, with molecular oxygen as the oxidant, research on the factors related to the selectivity is still rarely reported. As stated above, phenol is thermodynamically and kinetically more favourable to being further oxidized than benzene in the hydroxylation reaction of benzene to phenol, which makes the selectivity of phenol a challenge in this kind of continuous reaction.[21] Therefore, elucidating the factors affecting the selectivity is vitally important for the direct conversion of benzene to phenol.

Vanadium is the effective element for the hydroxylation of benzene to phenol with molecular oxygen as the oxidant. Various catalysts have been prepared to improve the yield and selectivity of phenol, including those with different species of vanadium oxide and supports.[22–27] Recently, we have developed a V_xO_y@C catalyst prepared from sucrose and NH_4VO_3 by a facile one-pot hydrothermal carbonization (HTC) method for the hydroxylation of benzene with molecular oxygen as the oxidant,[28] which exhibited good yield and selectivity of phenol. However, the mechanism and the factors related to the selectivity were not clear. Different catalytic performances are expected for a series of catalysts prepared from different carbon precursors because different types of biomass undergo different chemical reaction processes under the HTC conditions. In this work, various V_xO_y@C catalysts were prepared with different types of biomass to investigate the mechanism and the factors related to the selectivity.

Experimental section

Materials

The purchased chemicals were analytical grade and used without further purification. The water used was always deionized.

Preparation of the catalyst

The V_xO_y@C catalyst was prepared using a one-pot hydrothermal method, which was reproducible. To decrease the amount of NH_4VO_3 used in the preparation of the catalyst, the

College of Chemistry & Chemical Engineering, Shaanxi University of Science & Technology, Xi'an, Shaanxi, 710021, China. E-mail: wwt1806@163.com; mym63@sina.com

† Electronic supplementary information (ESI) available. See DOI: 10.1039/c6ra28768a

This journal is © The Royal Society of Chemistry 2017

Open Access Article. Published on 23 February 2017. Downloaded on 10/25/2025 7:37:09 PM.
This article is licensed under a Creative Commons Attribution 3.0 Unported Licence.

HTC temperature was 180 °C. Typically, NH_4VO_3 (0.05 g) and a desired amount of biomass were dissolved in distilled water (30 mL). The solution was stirred for a desired time, and transferred into a 50 mL Teflon-lined stainless steel autoclave, which was then sealed and heated at 180 °C for 24 h. The resulting products were filtered, washed several times with distilled water and finally dried at 100 °C overnight. These catalysts obtained from different types of biomass were denoted V_xO_y@C-*n*. The suffix *n* in V_xO_y@C-*n* represents the different types of biomass, of which the amount used in the hydrothermal method is listed in Table 1. All of the catalyst preparations were reproducible.

Characterization

The synthesized materials were characterized from X-Ray Diffraction (XRD) patterns obtained using an X-ray diffractometer (Rigaku IV) operated with Cu-K_α radiation at 40 kV and 40 mA. A Q45 environmental scanning electron microscope (SEM, USA) at 20 kV and 15 mA was used to study the sample morphology. An X-ray photoelectron spectrometer (XPS) was used at 15 kV and 8 mA. Fourier transform infrared (FT-IR) spectra were measured using a VERTEX 70 (Bruker, Britain) spectrometer with the KBr pellet technique in the range of 400 to 4000 cm^{-1}. Particle size analysis was achieved using a particle size surface potential analyzer (Malvern, Zetasizer Nano ZS90). The BET surface area of the catalyst was determined by adsorption of N_2 at −196 °C (instrument used: Gemini VII 2.00, Micromeritics Instrument Corporation). Thermogravimetric (TG) data were acquired using a thermoanalysis instrument (EXSTAR-6000, TG/TDA 6300) running under a nitrogen atmosphere with a temperature ramp of 10 °C min^{-1}. The loading content of V in the catalysts was determined using ICP-OES (Perkin Elmer, optima 7000DV).

Catalytic tests

The hydroxylation reaction was performed in a high pressure reactor consisting of a Teflon-lined stainless steel autoclave. Typically, 50 mg catalyst, 1.0 mL benzene, 3.0 mL acetonitrile and 0.8 g ascorbic acid were added to the reaction autoclave. Then, the reactor was charged with 3.0 MPa O_2 at room temperature. The hydroxylation reaction was carried out at a temperature of 80 °C under vigorous magnetic stirring. After a desired reaction time of 4 h, the solution was diluted to 25 mL in a volumetric flask. The concentrations of phenol in the solutions were measured using high performance liquid chromatography (HPLC, WAYEE LC 3000-2 Series instrument) using an Ultimate MB-C18 (250 mm × 4.60 mm) column with the UV detector at a wavelength of 254 nm. The terms of the reaction performance were calculated as follows:

$$\text{Conversion of benzene} = [(\text{initial moles of benzene} - \text{moles of residual benzene})]/(\text{initial moles of benzene}) \times 100\%;$$

$$\text{Selectivity} = (\text{moles of phenol produced})/(\text{conversion of benzene}) \times 100\%;$$

$$\text{Yield of phenol} = (\text{moles of phenol produced})/(\text{initial moles of benzene}) \times 100\%.$$

Adsorption of benzene and phenol

A certain amount of benzene (5.6 mmol) or phenol (5.3 mmol) and acetonitrile were mixed to form a solution. Then, 0.1500 g catalyst was added into the solution and the mixture was stirred at room temperature. The concentrations of benzene or phenol were analyzed using HPLC. The amount of benzene or phenol adsorbed on the catalyst was calculated as $q = [n_0 - c_tV]M/m$, where n_0 is the initial moles of benzene or phenol added to acetonitrile, c_t is the concentration of benzene or phenol after *t* minutes, *V* is the volume of the mixture, *M* is the molecular weight of benzene or phenol, *m* is the mass of catalyst added to the solution and *q* is the amount of benzene or phenol adsorbed.

Results and discussion

The amount of sucrose used for preparing the V_xO_y@C catalyst was 0.01 mol. Since one sucrose molecule could hydrolyze to one glucose molecule and one fructose molecule, the amount of glucose and fructose for preparing V_xO_y@C–G and V_xO_y@C–F, respectively, was 0.02 mol for both. The mixture of 0.01 mol glucose and 0.01 mol fructose was employed to obtain V_xO_y@C–(G + F). In this way, the equal molar carbon source of the different types of biomass including sucrose, glucose, fructose, and ascorbic acid was used to prepare the V_xO_y@C using the HTC (hydrothermal carbonization) method. The yield of

Table 1 Catalysts prepared from different types of biomass[a]

Entry	Catalyst	Biomass	Yield (g)	Average size[b] (nm)	V content[c] (wt%)	Surface area[d] (m^2 g^{-1})
1	V_xO_y@C–S	Sucrose (0.01 mol)	1.02	2292	1.2	2.37
2	V_xO_y@C–G	Glucose (0.02 mol)	0.97	1379	0.87	3.78
3	V_xO_y@C–F	Fructose (0.02 mol)	1.02	1577	1.1	2.88
4	V_xO_y@C–(G + F)	Glucose (0.01 mol) fructose (0.01 mol)	1.04	1421	1.1	2.25
5	V_xO_y@C–Vc	Ascorbic acid (0.02 mol)	0.99	1732	1.2	0.57

[a] V_xO_y@C was obtained from 0.05 g NH_4VO_3 and biomass at 180 °C for 24 h. [b] The average size was determined using a particle size surface potential analyzer. [c] The V content was determined using ICP-OES. [d] The surface area was determined from BET analysis.

Open Access Article. Published on 23 February 2017. Downloaded on 10/25/2025 7:37:09 PM.
This article is licensed under a Creative Commons Attribution 3.0 Unported Licence.

V_xO_y@C is shown in Table 1. The yield of the V_xO_y@C catalyst was nearly the same regardless of the kind of biomass employed as the carbon precursor. This indicated that the yield of the catalyst was not affected by the carbon source under the same hydrothermal carbonization (HTC) process.

The performance of the different V_xO_y@C catalysts in the hydroxylation reaction is shown in Table 2. The V_xO_y@C catalysts prepared from different types of biomass exhibited different catalytic performances. V_xO_y@C–G and V_xO_y@C–Vc exhibited higher conversion but lower selectivity. It can be found that V_xO_y@C–S gave the best yield and selectivity of phenol among the catalysts. These results indicated that the type of biomass influenced the polymerization and carbonization process during the HTC process for the catalyst preparation, which resulted in the different catalytic performances.

To investigate the reasons for the different catalytic performances, various characterization techniques were performed on the V_xO_y@C catalysts. The respective XRD patterns of the synthesized powders are shown in Fig. S1.† There was no difference in the XRD patterns of the different V_xO_y@C catalysts. A broad peak was found for the prepared catalyst, which was attributed to the irregularly oriented polycyclic aromatic carbon sheets of amorphous carbon. Mostly, the carbon materials or the M_xO_y@C materials obtained using the HTC method gave amorphous XRD spectra.[8,29] Vanadium oxides were not observed in the XRD spectra, due to their high dispersion and low content.

The Fourier transform infrared (FT-IR) spectra of all of the prepared catalyst samples were nearly identical (as shown in Fig. S2†). The O–H stretching bands were found at 3640 cm^{-1}, 3408 cm^{-1} and 3315 cm^{-1}. The bands at 1710 cm^{-1} and 1590 cm^{-1} were attributed to C=O and C=C vibrations, respectively, indicating the aromatization of the biomass during the hydrothermal treatment.

To investigate the thermal stability of the prepared catalysts, TG analysis was conducted. It was found (Fig. S3†) that the V_xO_y@C catalysts obtained from the different types of biomass exhibited similar weight loss during the heating process. The first weight loss below 100 °C was attributed to the adsorbed solvent (water) in the catalyst. The V_xO_y@C–G, V_xO_y@C–F, and V_xO_y@C–Vc catalysts had identical thermal stabilities. V_xO_y@C–(F + G) and V_xO_y@C–S had more adsorbed water in the catalyst. The weight loss at a temperature higher than 150 °C was attributed to the loss of the functional oxygen groups in the catalyst.

Table 2 The catalytic performance of the different V_xO_y@C[a] catalysts

Entry	Catalyst	Conversion (%)	Selectivity (%)	Yield (%)	TOF (h^{-1})
1	V_xO_y@C–S	9.7	96.0	9.3	23.2
2	V_xO_y@C–G	41.8	11.8	4.9	137.7
3	V_xO_y@C–F	10.1	82.8	8.4	26.3
4	V_xO_y@C–(F + G)	9.8	71.6	7.0	25.5
5	V_xO_y@C–Vc	31.7	21.8	6.9	75.7
6	V_xO_y@C–S[b]	—	—	Trace	—
7	—[c]	—	—	Trace	—
8	V_xO_y@C–S[d]	9.4	98.7	9.3	22.4
9	V_xO_y@C–S[e]	32.9	26.1	8.6	—
10	V_xO_y@C–S[f]	37.3	18.1	6.7	—
11	V_xO_y@C–S[g]	—	—	Trace	—
12	C–S[h]	1.4	>99	1.4	—
13	C–G[h]	2.0	67.4	1.4	—
14	C–Vc[h]	1.4	>99	1.4	—

[a] Reaction conditions: catalyst, 50 mg; ascorbic acid, 0.8 g; acetonitrile, 3.0 mL; benzene, 1.0 mL; O_2 pressure, 3.0 MPa; temperature, 80 °C; reaction time 4 hours. [b] Without ascorbic acid. [c] Without catalyst; only ascorbic acid was employed as the catalytic system. [d] Benzene was replaced with deuterated benzene (C_6D_6). [e] With 2.0 mmol TEMPO added. [f] With 4.0 mmol TEMPO added. [g] With 30 mg 2,6-di-*tert*-butyl-4-methylphenol (BHT) added. [h] Bare carbon used as the catalyst obtained from biomass. TOF: turn-over-frequency (moles of benzene converted per mole of V in the catalyst per hour).

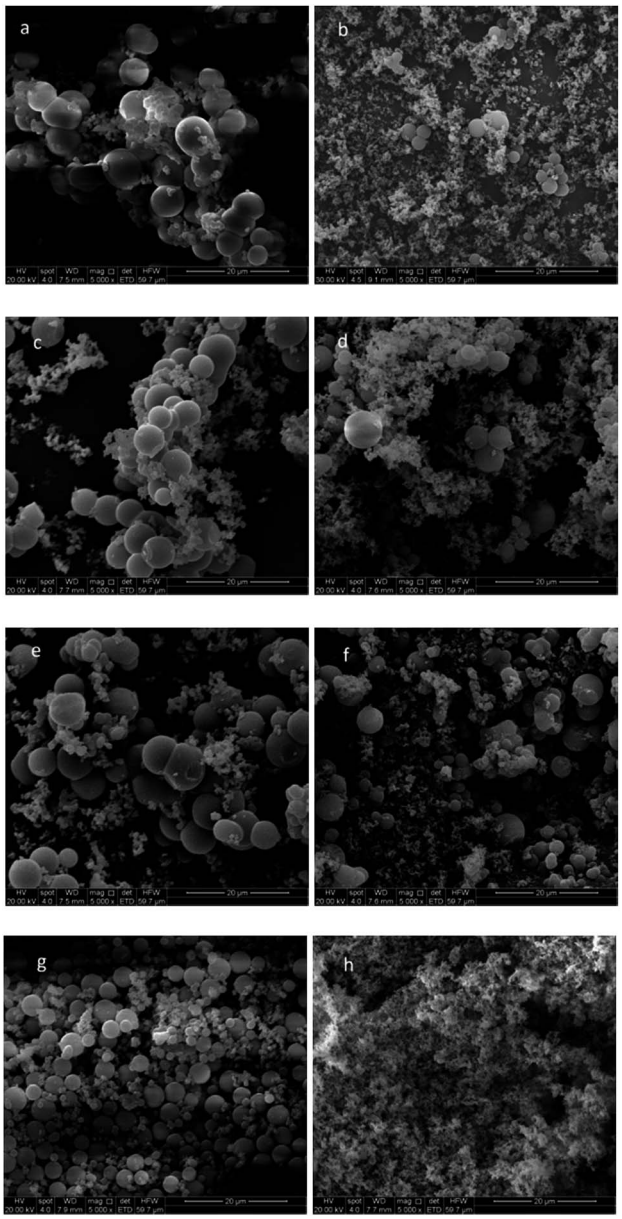

Fig. 1 SEM images of the catalysts. (a) V_xO_y@C–S, (b) V_xO_y@C–G, (c) V_xO_y@C–F, (d) V_xO_y@C–(F + G), (e) V_xO_y@C–Vc, (f) V_xO_y@C–starch, (g) V_xO_y@C–furfural and (h) V_xO_y@C–HMF.

Open Access Article. Published on 23 February 2017. Downloaded on 10/25/2025 7:37:09 PM.
This article is licensed under a Creative Commons Attribution 3.0 Unported Licence.

The prepared samples exhibited a spherical particle morphology as evidenced by the SEM images shown in Fig. 1. The V_xO_y@C catalyst contained two kinds of sphere regardless of the kind of biomass employed. One was an isolated large microsphere; the other was an interconnected smaller sphere. To investigate the details, the HTC time was varied to obtain the V_xO_y@C catalysts, as shown in Fig. 2. With an increase of the HTC time, there were still two kinds of microsphere, which indicated that the two kinds of microsphere formed through different mechanisms. To further study the mechanism, starch, 5-hydroxymethylfurfural (HMF, a dehydration product of glucose or fructose) and furfural were selected as the carbon precursor sources. It can be noted that two kinds of microspheres were obtained with starch (Fig. 1f). However, a uniform morphology was obtained with furfural and HMF, as shown in Fig. 1g and h. Particularly, the small uniform microspheres obtained were similar to the smaller microspheres in Fig. 1a–f. This indicated that the small spheres were mainly formed from HMF which was generated by hydrolysis of the biomass. Hydrolysis of polysaccharide occurred, which was followed by the dehydration and polymerization of monosaccharide or HMF, and then the carbonization process to form the spherical morphology embedded vanadium oxides.[28]

The particle size distributions of the different V_xO_y@C catalysts are presented in Fig. 3. According to the figures, similar trends in the particle size distributions were found. V_xO_y@C–F showed the narrowest particle size distribution area while V_xO_y@C–(F + G) gave the broadest. The average sizes are presented in Table 1. It was noted that V_xO_y@C–S exhibited the largest average size. V_xO_y@C–(F + G) gave a size between the sizes of V_xO_y@C–F and V_xO_y@C–G. These results indicate that the biomass precursor affected the polymerization and carbonization under hydrothermal conditions. Although sucrose would hydrolyze in the water under the reaction conditions, it was not fully hydrolysed. Otherwise, V_xO_y@C–S and V_xO_y@C–(F + G) would have the same particle size and catalytic performance. Therefore, the polysaccharide hydrolyzed to disaccharides or monosaccharides, which polymerized and partially carbonized to form the bigger spheres while the HMF formed from the fructose/glucose polymerized and partially carbonized to form the smaller spheres.

To investigate the detailed surface functionality, XPS was performed. The V2p spectra of the catalysts are presented in Fig. 4. The V2p spectra of the catalysts can be deconvoluted into V^{5+}, V^{4+} and V^{3+}. The peaks at 517.4–518.0 eV were ascribed to the V^{5+} species and the peaks at 516.0–516.9 eV were recognized as arising from the V^{4+} species, while the peaks at 514.4–515.3 eV were attributed to the V^{3+} species.[12,30,31] It can be found that the V species were varied in the different catalysts, which indicated that the different biomass precursors affected the vanadium oxide formation. Three kinds of V species existed in V_xO_y@C–S and V_xO_y@C–(F + G). Both V^{5+} and V^{3+} species were found in V_xO_y@C–F. There was no V^{5+} observed in V_xO_y@C–G or V_xO_y@C–Vc, but both of them showed the existence of V^{4+} and V^{3+}. It has been reported that V^{4+} contributes more to the activity of a V catalyst for the hydroxylation of benzene to phenol.[32,33] The greater content of the V^{4+} and V^{3+} species in the V_xO_y@C–G and V_xO_y@C–Vc catalysts (Table S1†) contributed to their high activities.

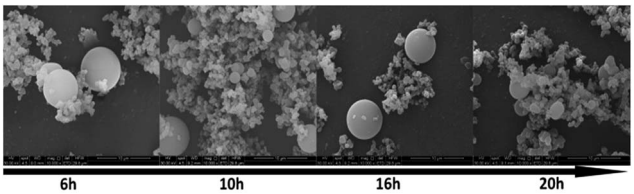

Fig. 2 The SEM images of V_xO_y@C–S formed with different HTC times.

The C1s peak was deconvoluted into several peaks at the binding energy values of 284.6 eV, 285.4–286.7 eV, 287.0–287.7 eV, 288.3–289.0 eV and 290.7–291.4 eV, corresponding to aliphatic and/or aromatic groups (C–H_x and C–C/C=C), alcohol and/or ether groups (–C–O), carbonyl groups (>C=O), carboxyl and/or ester groups (O=C–O–), and shake-up satellite peaks due to π–π* transitions,[34,35] respectively (Fig. S4†). The changes in the carbon species with the use of different biomass precursors indicated the different polymerization and carbonization reactions that occurred during the HTC process.

The O/C molar ratio was calculated from the XPS data, and is shown in Table 3. The O/C molar ratio was usually in the range of 0.26–0.36 for the carbon materials obtained using the HTC method with the biomass types such as sucrose, glucose, and fructose used as the precursors.[36–39] However, the prepared V_xO_y@C gave a higher O/C ratio, as high as 0.62–0.87. This indicated that the O/C ratio was greatly increased due to the formation of V_xO_y oxides in the carbonaceous microspheres.

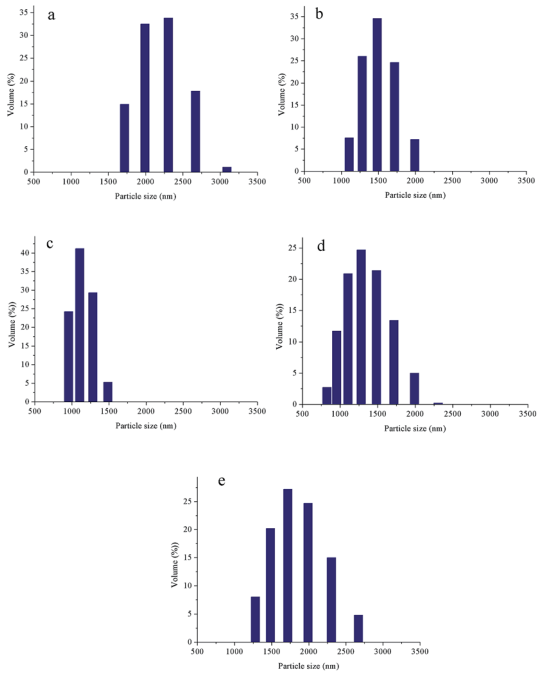

Fig. 3 Particle size distributions of the V_xO_y catalysts. (a) V_xO_y@C–S, (b) V_xO_y@C–G, (c) V_xO_y@C–F, (d) V_xO_y@C–(F + G) and (e) V_xO_y@C–Vc.

Open Access Article. Published on 23 February 2017. Downloaded on 10/25/2025 7:37:09 PM.
This article is licensed under a Creative Commons Attribution 3.0 Unported Licence.

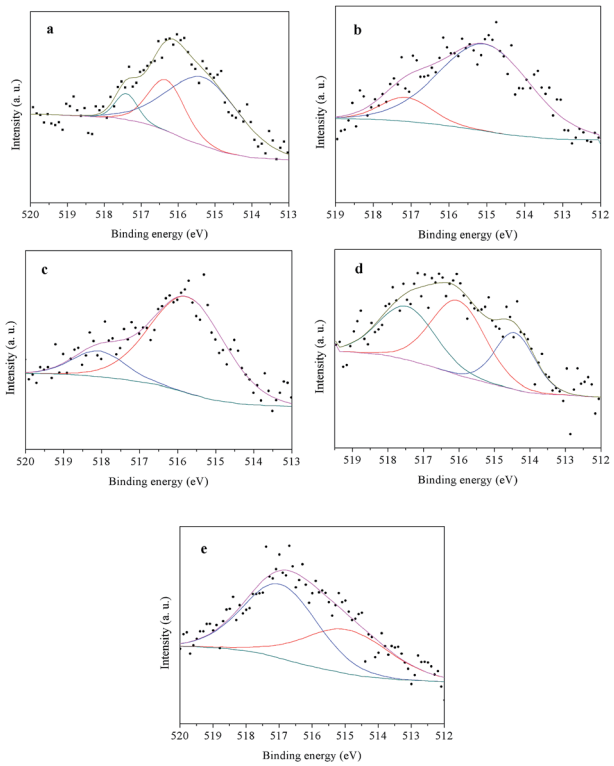

Fig. 4 V2p spectra of the catalysts. (a) V_xO_y@C–S, (b) V_xO_y@C–G, (c) V_xO_y@C–F, (d) V_xO_y@C–(F + G) and (e) V_xO_y@C–Vc.

It can be observed that the C1 species content (graphitic carbon, C–C and C–H_x) increased in the order V_xO_y@C–S > V_xO_y@C–F > V_xO_y@C–(F + G) > V_xO_y@C–G, which coincided with the increase of the phenol yield (Table 2, entries 1–4, and Fig. S5†). The higher C1 species content could lead to the possibility of a higher content of defect active sites such as the armchair type which have a positive effect on the yield of phenol.[18] Besides the V species on the catalyst, one may postulate that the conversion of benzene was probably related to the C3 species since V_xO_y@C–G and V_xO_y@C–Vc had a high C3 species content and high TOF. Furthermore, it was reported that phenylboronic acid can be oxidized to phenol in a menadione–ascorbate–O_2 system.[40] This implied that the activity was probably related to the quinoid species in the C3 species. To test this postulation, quinones were added to the reaction system, the results of which are shown in Table 4. With the quinones added, the activity was not enhanced, but the activity and selectivity of phenol were decreased. This implied that the high activity of V_xO_y@C–G and V_xO_y@C–Vc was not related to the quinoid species on the catalyst but the selectivity was related to the quinoid species on the catalyst.

Table 4 The catalytic performance of the different quinone additives[a]

Entry	Quinine additives	Conversion (%)	Selectivity (%)	Yield (%)
1	Menadione	10.5	90.9	9.6
2	Benzoquinone	9.1	60.0	5.5
3	9,10-Anthraquinone	8.8	71.6	6.3
4	9,10-Anthraquinone[b]	2.2	69.8	1.6

[a] Reaction conditions: V_xO_y@C–S catalyst, 50 mg; quinone additives, 30 mg; ascorbic acid, 0.8 g; acetonitrile, 3.0 mL; benzene, 1.0 mL; O_2 pressure, 3.0 MPa; temperature, 80 °C; reaction time, 4 hours. [b] Without V_xO_y@C–S catalyst; ascorbic acid and anthraquinone were employed as the catalytic system.

Ascorbic acid and quinone can lead to quinone redox cycling to generate reactive oxygen,[40] which may overoxidize phenol and decrease the selectivity. However, when anthraquinone and ascorbic acid were employed as the catalytic system, the conversion of phenol was not increased, but was decreased to the level for anthraquinone as the catalyst (Table 5, entries 2–4), which indicated that the quinone groups could not assist the ascorbic acid to oxidize phenol, but consumed the ascorbic acid, reducing the activity of the ascorbic acid. When ascorbic acid was employed as the catalyst, the conversion of phenol reached 77.8%, which indicated that ascorbic acid could activate oxygen to oxidize phenol (Table 5, entry 2). However, the active oxygen species generated by the ascorbic acid could not attack the benzene ring (Table 2, entry 7). V_xO_y@C–S could not generate active oxygen (Table 2, entry 6) to attack the benzene ring. Therefore, the active oxygen was generated by V_xO_y@C–S and ascorbic acid, which then attacked the benzene ring to form phenol.

To investigate the mechanism, the kinetic isotope effect (KIE) was studied. When the hydroxylation reaction was examined with benzene-d_6, there was no KIE ($k_H/k_D = 1.0$) observed (Table 2, entries 1 and 8), which indicated that C–H activation in the benzene ring was not the rate-determining step.[41] Therefore, the activation of molecular oxygen may be the rate-determining step.[42] When the radical scavenger of BHT (2,6-di-*tert*-butyl-4-methylphenol) was added, no reaction happened (Table 2, entry 11), which indicated the participation of hydroxyl radicals

Table 3 Summary of the XPS C1s data of the catalysts

Entry	Catalyst	C1 C–H_x, C–C, C=C	C2 –C–O	C3 >C=O	C4 O=C–O–	C5 π–π* transition	O/C
1	V_xO_y@C–S	284.6, 54.7%	286.1, 28.3%	287.0, 3.3%	288.4, 13.6%	—	0.73
2	V_xO_y@C–G	284.6, 33.8%	285.6, 18.6%	287.5, 47.6%	—	—	0.62
3	V_xO_y@C–F	284.6, 44.0%	286.7, 49.9%	—	289.0, 3.92%	290.7, 2.18%	0.74
4	V_xO_y@C–(F + G)	284.6, 40.2%	285.7, 47.2%	—	288.3, 12.6%	—	0.63
5	V_xO_y@C–Vc	284.6, 25.4%	285.4, 31.2%	287.7, 42.1%	—	291.36, 1.25%	0.87

Open Access Article. Published on 23 February 2017. Downloaded on 10/25/2025 7:37:09 PM.
This article is licensed under a Creative Commons Attribution 3.0 Unported Licence.

Table 5 The conversion of phenol with different catalytic systems[a]

Entry	Additives	Conversion (%)
1	None	12.3
2	Ascorbic acid	77.8
3	9,10-Anthraquinone	14.5
4	Ascorbic acid + 9,10-anthraquinone	14.5
5	V_xO_y@C–S	24.5
6	V_xO_y@C–S + ascorbic acid	62.3
7	V_xO_y@C–S + ascorbic acid + 9,10-anthraquinone	63.5

[a] Reaction conditions: phenol, 1.1 mmol; acetonitrile, 3.0 mL; O_2 pressure, 3.0 MPa; temperature, 80 °C; reaction time, 4 hours.

in the reaction. Moreover, the formation of H_2O_2 was detected in the reaction by redox titration with $KMnO_4$.[43] It can be deduced that ascorbic acid can help V_xO_y@C–S to generate active oxygen species and H_2O_2. With the help of the catalyst, the formed H_2O_2 could produce the hydroxyl radical which attacked benzene to form phenol. Furthermore, the conversion of benzene was increased when TEMPO was added (Table 2, entries 9 and 10). The added TEMPO could increase the reaction rate by generating the ascorbic acid radical with reaction of TEMPO and ascorbic acid,[44] which can generate more active oxygen species by activating molecular oxygen and lead to more H_2O_2 formation. Therefore, more available hydroxyl radicals can attack benzene, improving the activity. However, too many hydroxyl radicals can also oxidize phenol to form overoxidation products, leading to a decline in the selectivity.

Besides the oxidation of phenol being able to influence the selectivity of phenol, the adsorption of phenol on the catalyst can also affect the selectivity.[45] The equation for the selectivity of cyclohexene in the partial hydrogenation of benzene reaction could be employed to illustrate the selectivity of phenol in the hydroxylation of benzene to phenol.[46] The equation is as follows:

$$S_{(\text{phenol})} = \frac{r_{\text{des}} - r_{\text{ads}}}{r_{\text{O}}}$$

r_{des} is the rate of desorption of the formed phenol; r_{ads} is the rate of re-adsorption of the phenol; r_{O} is the oxidation rate of phenol. The equation illustrates the factors relating to the selectivity. When the amount of hydroxyl radical increased, the oxidation rate of phenol (r_{O}) would be increased, therefore, the

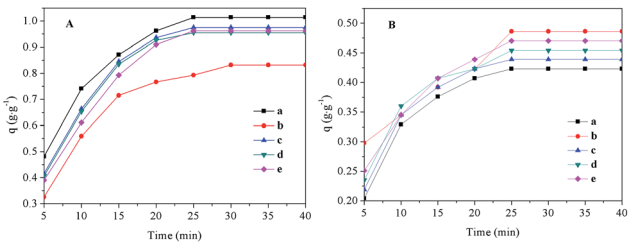

Fig. 5 Adsorption of (A) benzene and (B) phenol. (a) V_xO_y@C–S (■), (b) V_xO_y@C–G (●), (c) V_xO_y@C–F (▲), (d) V_xO_y@C–(F + G) (▼) and (e) V_xO_y@C–Vc (◆).

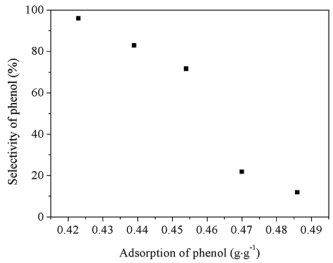

Fig. 6 The relationship between the adsorption of phenol and selectivity of phenol.

selectivity will be decreased. In addition, it can be seen in the equation that the adsorption of phenol affects the selectivity of phenol. Higher adsorption of phenol disfavored the selectivity of phenol.

The adsorption of benzene or phenol on different V_xO_y@C catalysts is shown in Fig. 5. The adsorption of benzene or phenol reached equilibrium after about 25 minutes. For the adsorption of benzene, V_xO_y@C–G had the lowest adsorption of benzene while V_xO_y@C–S showed the highest adsorption of benzene. V_xO_y@C–F, V_xO_y@C–(F + G), and V_xO_y@C–Vc gave similar amounts of adsorbed benzene. The adsorption of benzene could not be associated with the activity, as the C–H in the benzene ring was not the rate-determining step. Furthermore, the hydroxylation of benzene to phenol reaction was first order in oxygen and zero order in benzene.[42]

For the adsorption of phenol, the adsorbed amount followed the order V_xO_y@C–G > V_xO_y@C–Vc > V_xO_y@C–(F + G) > V_xO_y@C–F > V_xO_y@C–S. The adsorbed amount of phenol was consistent with the selectivity of phenol, as shown in Fig. 6. The high C–H_x and C–C/C=C content on the surface would increase the hydrophobicity of the catalyst, leading to the decrease of the adsorption of phenol. The higher adsorption of phenol indicated the stronger interaction between the catalyst and phenol, which would reduce the desorption of formed phenol on the catalyst surface and enhance the re-adsorption of phenol. This would result in a decline in the selectivity. Therefore, it can be deduced that the adsorption of phenol affected the selectivity of phenol in the hydroxylation reaction.

Conclusions

During the HTC process, the biomass undergoes a hydrolysis–polymerization–carbonization process, which is affected by the type of biomass precursor. V_xO_y@C–S showed the best catalytic performance for the reaction of hydroxylation of benzene to phenol among the V_xO_y@C series. Insight into the mechanism of the hydroxylation of benzene was found; with the help of ascorbic acid, the V species can activate molecular oxygen to form the active oxygen species which attacks benzene to form phenol. The activity of the catalyst mainly depended on the V species on the catalyst. The selectivity of phenol was related to the adsorption of phenol and the oxidation rate of phenol. The low adsorption of phenol and slow oxidation rate of phenol were favorable for a good selectivity of phenol.

Open Access Article. Published on 23 February 2017. Downloaded on 10/25/2025 7:37:09 PM.
This article is licensed under a Creative Commons Attribution 3.0 Unported Licence.

Acknowledgements

The authors thank greatly the National Natural Science Foundation of China (21403136), China Postdoctoral Science Foundation (2015M72514) and Natural Science Basic Research Plan in Shaanxi Province of China (2016JQ2025) for financial support.

Notes and references

1 H. Yuzawa and H. Yoshida, *Chem. Commun.*, 2010, **46**, 8854–8856.
2 M. Yamada, K. Karlin and S. Fukuzumi, *Chem. Sci.*, 2016, **7**, 2856–2863.
3 S. S. Acharyya, S. Ghosh and R. Bal, *Chem. Commun.*, 2014, **50**, 13311–13314.
4 T. Yu, Q. Zhang, S. Xia, G. Li and C. Hu, *Catal. Sci. Technol.*, 2014, **4**, 639–647.
5 P. Borah and A. Datta, *Appl. Catal., A*, 2010, **376**, 19–24.
6 K. Kamata, T. Yamaura and N. Mizuno, *Angew. Chem., Int. Ed.*, 2012, **51**, 7275–7278.
7 K. Tian, W.-J. Liu, S. Zhang and H. Jiang, *Green Chem.*, 2016, **18**, 5643–5650.
8 Y. Ma, X. Ren, W. Wang, P. Lu and L. Shi, *React. Kinet., Mech. Catal.*, 2016, **117**, 693–702.
9 X. Cai, Q. Wang, Y. Liu, J. Xie, Z. Long, Y. Zhou and J. Wang, *ACS Sustainable Chem. Eng.*, 2016, **4**, 4986–4996.
10 A. Tabler, A. Häusser and E. Roduner, *J. Mol. Catal. A: Chem.*, 2013, **379**, 139–145.
11 M. Tani, T. Sakamoto, S. Mita, S. Sakaguchi and Y. Ishii, *Angew. Chem., Int. Ed.*, 2005, **44**, 2586–2588.
12 X. Gao and J. Xu, *Catal. Lett.*, 2006, **111**, 203–205.
13 Z. Long, Y. Zhou, G. Chen, W. Ge and J. Wang, *Sci. Rep.*, 2014, **4**, 3651.
14 Y. Liang, X. Li, X. Wang, Y. Yan, P. Feng and N. Jiao, *ACS Catal.*, 2015, **5**, 1956–1963.
15 S.-t. Yamaguchi, S. Sumimoto, Y. Ichihashi, S. Nishiyama and S. Tsuruya, *Ind. Eng. Chem. Res.*, 2005, **44**, 1–7.
16 S. Shang, B. Chen, L. Wang, W. Dai, Y. Zhang and S. Gao, *RSC Adv.*, 2015, **5**, 31965–31971.
17 S. Fukuzumi and K. Ohkubo, *Asian J. Org. Chem.*, 2015, **4**, 836–845.
18 G. Wen, S. Wu, B. Li, C. Dai and D. S. Su, *Angew. Chem., Int. Ed.*, 2015, **54**, 4105–4109.
19 J. Xu, H. Liu, R. Yang, G. Li and C. Hu, *Chin. J. Catal.*, 2012, **33**, 1622–1630.
20 J. Yang, G. Sun, Y. Gao, H. Zhao, P. Tang, J. Tan, A. Lu and D. Ma, *Energy Environ. Sci.*, 2013, **6**, 793–798.
21 B. Cornils and W. A. Herrmann, *J. Catal.*, 2003, **216**, 23–31.
22 C. Guo, W. Du, G. Chen, L. Shi and Q. Sun, *Catal. Commun.*, 2013, **37**, 19–22.
23 Y.-k. Masumoto, R. Hamada, K. Yokota, S. Nishiyama and S. Tsuruya, *J. Mol. Catal. A: Chem.*, 2002, **184**, 215–222.
24 L. Zhao, Y. Dong, X. Zhan, Y. Cheng, Y. Zhu, F. Yuan and H. Fu, *Catal. Lett.*, 2012, **142**, 619–626.
25 Y. Bao, H. Jiang, W. Xing, R. Chen and Y. Fan, *React. Kinet., Mech. Catal.*, 2015, **115**, 535–547.
26 X. Chen, F. Wang and J. Xu, *Top. Catal.*, 2011, **54**, 1016–1023.
27 L. Hu, C. Wang, B. Yue, X. Chen and H. He, *RSC Adv.*, 2016, **6**, 87656–87664.
28 W. Wang, G. Ding, T. Jiang, P. Zhang, T. Wu and B. Han, *Green Chem.*, 2013, **15**, 1150–1154.
29 G. Yu, B. Sun, Y. Pei, S. Xie, S. Yan, M. Qiao, K. Fan, X. Zhang and B. Zong, *J. Am. Chem. Soc.*, 2009, **132**, 935–937.
30 X. Gao, X. Lv and J. Xu, *Kinet. Catal.*, 2010, **51**(3), 394–397.
31 S. Nordlinder, A. Augustsson, T. Schmitt, J. Guo, J. Nordgren, T. A. Gustafsson and K. Edström, *Chem. Mater.*, 2003, **15**(15), 3227–3232.
32 W. Ge, Z. Long, X. Cai, Q. Wang, Y. Zhou, Y. Xu and J. Wang, *RSC Adv.*, 2014, **4**, 45816–45822.
33 E. Battistel, R. Tassinari, M. Fornaroli and L. Bonoldi, *J. Mol. Catal. A: Chem.*, 2003, **202**, 107–115.
34 S. Biniak, G. Szymański, J. Siedlewski and A. Ś. j. m. tkowski, *Carbon*, 1997, **35**, 1799–1810.
35 L. Yu, C. Falco, J. Weber, R. J. White, J. Y. Howe and M.-M. Titirici, *Langmuir*, 2012, **28**, 12373–12383.
36 J. Ryu, Y.-W. Suh, D. J. Suh and D. J. Ahn, *Carbon*, 2010, **48**, 1990–1998.
37 M. Sevilla and A. Fuertes, *Carbon*, 2009, **47**, 2281–2289.
38 M. Sevilla and A. B. Fuertes, *Chem.–Eur. J.*, 2009, **15**, 4195–4203.
39 C. Falco, F. P. Caballero, F. Babonneau, C. Gervais, G. Laurent, M. M. Titirici and N. Baccile, *Langmuir*, 2011, **27**, 14460–14471.
40 S. D. Gastón, D. M. Monzón, F. P. Crisóstomo, M. Tomás, V. S. Martín and C. Romen, *Chem. Commun.*, 2015, **51**, 7027–7030.
41 L. Wu, W. Zhong, B. Xu, Z. Wei and X. Liu, *Dalton Trans.*, 2015, **44**, 8013–8020.
42 Y. Gu, X. Zhao, G. Zhang, H. Ding and Y. Shan, *Appl. Catal., A*, 2007, **328**, 150–155.
43 Y. Shiraishi, S. Kanazawa, Y. Kofuji, H. Sakamoto, S. Ichikawa, S. Tanaka and T. Hirai, *Angew. Chem., Int. Ed.*, 2014, **53**, 13454–13459.
44 H. Yang, J. Chen, J. Li, Y. Lv and S. Gao, *Appl. Catal., A*, 2012, **415–416**, 22–28.
45 W. Wang, M. Yao, Y. Ma and J. Zhang, *Prog. Chem.*, 2014, **26**, 1665–1672.
46 J. Struijk, M. d'Angremond, W. J. F. Regt and J. J. F. Scholten, *Appl. Catal., A*, 1992, **83**, 263–295.

 This journal is © The Royal Society of Chemistry 2017